

## ANNOUNCEMENT

---

### The 2005 François Naftali Frenkiel Award for Fluid Mechanics

The recipient of the 22nd François Naftali Frenkiel Award for Fluid Mechanics is **Roberto Verzicco**, Politecnico di Bari in Italy, for his paper “Effects of nonperfect thermal sources in turbulent thermal convection,” which was published in *Physics of Fluids*, Vol. 16, pp. 1965–1979 (2004). Professor Verzicco was presented with this award on 20 November 2005 at the annual meeting of the APS Division of Fluid Dynamics in Chicago, Illinois. He received a check for \$1000 plus a scroll bearing the following citation:

Judicious use of numerical simulations to resolve apparent discrepancies in experimental studies of the scaling behavior of high Rayleigh number convection by clarifying the dynamic role of the boundaries in heat transfer.

The purpose of this Award, which is named after Dr. F. N. Frenkiel, founder and longtime editor of *Physics of Fluids*, is to recognize significant contributions in fluid mechanics by young investigators. The Award is sponsored by the Division of Fluid Dynamics of the APS, and is given annually to a young author of a paper that has been published in *Physics of Fluids*, during the calendar year preceding the presentation. “Young” will normally be defined as being under 40 years of age. More than one author may be involved, and one author may be a thesis advisor sharing the Award if he/she is also under 40. The winner of this Award is selected by a committee appointed by the Chair of the Division of Fluid Dynamics of the APS.



**Roberto Verzicco** received his Ph.D. in Fluid Dynamics in 1993 at the Università di Roma “La Sapienza” with a thesis on azimuthal instabilities of viscous vortex rings under the supervision of Professor Paolo Orlandi. He joined in 1993 the Department of Mechanics and Aeronautics of Università di Roma “La Sapienza” as researcher. In 1998 he became associate professor at the Department of Mechanical and Management Engineering (DIMEG) and Excellence Center of Computational Mechanics (CEMeC) of Politecnico di Bari where he became full professor in 2003. His research activities are mainly in numerical simulation of classical and buoyancy driven turbulence, flows in complex geometries using the immersed boundary method, and large eddy simulation.

---

**François Naftali Frenkiel**, who was born in Warsaw, Poland, on 19 September 1910, received his undergraduate education in Mechanical and Aeronautical Engineering at the University of Ghent, Belgium, and his Ph.D. in Physics from the University of Lille in France where he studied under the direction of Kampé de Fériet. He came to the States in 1947 and was associated successively with Cornell University, the U.S. Naval Ordnance Laboratory, the Johns Hopkins University Applied Physics Laboratory, and, from 1960 until his retirement, with the David W. Taylor Naval Ship Research and Development Center. In addition to being the founder and longtime editor of *Physics of Fluids*, he served on a large number of national and international committees, e.g., to name but a few, the International Union of Theoretical and Applied Mechanics, the U.S. National Committee on Theoretical and Applied Mechanics, and the Division of Fluid Dynamics of the American Physical Society of which he was the chairman and secretary on numerous occasions. He published extensively in the field of turbulent flows and pioneered the application of high-speed digital computing methods to the measurement of turbulence and the mathematical modeling of urban pollution. He was elected Fellow of the American Physical Society, the American Geophysical Union, and the American Association for the Advancement of Science. Dr. Frenkiel retired in 1981 and passed away on 9 July 1986, in Washington, D.C.

# Effects of nonperfect thermal sources in turbulent thermal convection

R. Verzicco<sup>a)</sup>

*Politecnico di Bari, DIMeG and CEMeC, Via Re David 200, 70125, Bari, Italy*

(Received 21 July 2003; accepted 5 March 2004; published online 30 April 2004)

The effects of the plates thermal properties on the heat transfer in turbulent thermal convection are investigated by direct numerical simulations of the Navier–Stokes equations with the Boussinesq approximation. It has been found that the governing parameter is the ratio of the thermal resistances of the fluid layer  $R_f$  and the plates  $R_p$ ; when this ratio is smaller than a threshold value ( $R_f/R_p \approx 300$  arbitrarily defined by requiring that the actual heat transfer differs by less than 2% from its ideal value), the finite conductivity of the plates limits the heat transfer in the cell. In addition, since  $R_f$  decreases for increasing Rayleigh numbers, any experimental apparatus is characterized by a threshold Rayleigh number that cannot be exceeded if the heat transfer in the cell has not to be influenced by the thermal properties of the plates. It has been also shown that the plate effects cannot be totally corrected by subtracting the temperature drop occurring within the plates from the measured total temperature difference. This is due to the changes produced in the thermal plume dynamics by the reduced local heat flux at the plate/fluid interface. A model with a correction factor has been derived to account for the plates effects and it gave the appropriate correction for a recent experiment in which the heat transfer measurements were systematically smaller than a theoretical prediction. In view of the present correction the discrepancy between theory and experiments addressed by Nikolaenko and Ahlers [Phys. Rev. Lett. **91**, 084501 (2003)] can be therefore resolved. The application of the proposed correction to the results in the literature can also reconcile the heat transfer measurements for water and mercury that appear systematically smaller than in other fluids.

© 2004 American Institute of Physics. [DOI: 10.1063/1.1723463]

## I. CONTEXT AND MOTIVATION

Turbulent thermal convection is one of the problems attracting most of the interest in fluid dynamics owing to the physical richness of the phenomena and the involved technical and geophysical applications. The cooling of electronic components (mainly microprocessors) is in fact the major factor limiting the increase of their operational frequency while the differential heating of the ocean and atmosphere is the driving engine for large-scale circulations. On the other hand, from the physical viewpoint, thermal convection is interesting *per se* since it provides a paradigm of complex dynamics within relatively simple and controllable setups. It has recently been observed, however, that some experiments performed under apparently similar conditions do not show identical dynamics (Refs. 1–5, only to mention a few experiments performed in a slender cylindrical cell) and, since the cell shape and the main nondimensional parameters are in the same range, it has been conjectured that the temperature boundary conditions might cause the differences.<sup>6,7</sup> In particular, one of the most controversial points is the appearance of the ultimate regime<sup>8</sup> which may have been observed in some experiments but not in others. In this regime, the transferred heat current should increase as  $\Delta_T^{3/2}$  (apart from logarithmic corrections) being  $\Delta_T$  the imposed temperature difference. Given the extreme dynamics characterizing this

regime (ultrahard turbulence and “ballistic” plumes) experimentalists push their apparatus to the limits with the aim of reaching the highest Rayleigh number and this can introduce some uncertainty in the results.

A typical setup is made of two horizontal parallel plates kept at a distance  $h$  and maintained at different temperatures; the working fluid is vertically confined by the plates and horizontally by a lateral wall. When a temperature difference  $\Delta_T$  is established between the horizontal surfaces (if  $\Delta_T$  exceeds a critical value and the lower temperature is warmer than the upper) the fluid starts moving because of buoyancy forces. The role of the side wall is to confine the working fluid and to thermally insulate it from the external ambient; as a consequence this wall is made of poorly thermal conducting material and its thickness is kept as small as possible (0.01%–0.1% of the plates distance  $h$ ) in order to prevent the heat leakage. The horizontal plates, on the contrary, must maintain a uniform temperature distribution at the solid/fluid interface and must allow the transit of the imposed heat current producing a negligible temperature drop across their thickness; these plates, therefore, are thick solid blocks of highly thermal conducting metals (usually pure copper) whose large thickness (5%–15% of the plates distance  $h$ ) serves also as heat capacity for the flow. In reality, the choice of the plate thickness is a trade off between several parameters like the thermal homogeneity at the fluid solid interface, the global time response of the plate and the local heat capacity.

In laboratory experiments, for every imposed heat cur-

<sup>a)</sup>Telephone: +39 0805963898; fax: +39 0805963411; electronic mail: verzicco@poliba.it

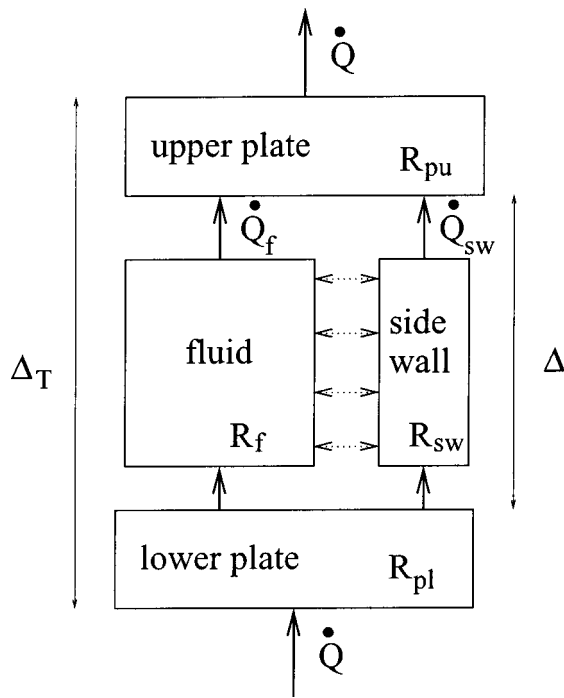


FIG. 1. Schematic of the electrical analogue of the convection cell. The dotted arrows between the fluid and the side wall indicate the weak thermal coupling. Any other heat leakage is neglected since thermal shields are usually placed around the cell and, given the low mean temperatures, the radiation can be safely neglected.

rent  $\dot{Q}$  a temperature difference  $\Delta_T$  is measured which in nondimensional form, respectively, read

$$Nu = \frac{\dot{Q}h}{\lambda_f \Delta_T S} \quad \text{and} \quad Ra = \frac{g \alpha_f \Delta_T h^3}{\nu_f k_f}, \quad (1)$$

with  $g$ ,  $\alpha_f$ ,  $\nu_f$ , and  $k_f$  the acceleration of gravity, the isobaric thermal expansion coefficient of the fluid, its kinematic viscosity, and thermal diffusivity.  $S$  is the wetted plate surface, and  $\lambda_f$  the fluid thermal conductivity related to  $k_f$  through  $k_f = \lambda_f / (\rho_f C_{pf})$ , being  $\rho_f$  the mean fluid density and  $C_{pf}$  its isobaric specific heat.

If we make an electrical analog of the convection cell we can think of the heat current as an electrical current and the temperature difference as a potential difference. In this context each component of the cell can be concentrated in a single element interested by a heat current and across which a temperature drop occurs. The side wall, in principle, should allow neither a heat flux nor a thermal coupling with the fluid. On the other hand, since in laboratory experiments the plates temperature is measured somewhere within the plate thickness and the same value is retained at the plate/fluid interface, it is assumed that the temperature drop inside the plates is negligible ( $\Delta \approx \Delta_T$  in Fig. 1). It is worth mentioning that in some experiments, especially those involving liquid metals, the measured temperature difference  $\Delta_T$  is corrected by subtracting the temperature drop within the plates estimated by the pure conducting temperature profiles or extrapolated by temperature measurements at two different depths in the plates. This, however, would imply that the plates effect could be totally accounted by a correction of  $\Delta_T$

while the present results will show that this is not the case. If, in analogy with Ohm's law, we write  $\Delta_i = R_i \dot{Q}_i$  (with  $R_i$  the thermal resistance of the  $i$ th cell component) the above requirements are equivalent to  $R_{pl} \ll R_f$ ,  $R_{pu} \ll R_f$ , and  $R_{sw} \gg R_f$ . Because of the thermal convection, however, the thermal resistance of the fluid layer  $R_f$  continuously decreases for increasing  $\Delta$  (or  $\Delta_T$ ) and the previous conditions cannot be both maintained for every value of  $\Delta$ .

In particular, several recent papers<sup>9-11</sup> have shown that in low aspect ratio cells for Rayleigh numbers  $Ra \leq 10^{11}$  the heat leakage through the side wall was not always negligible with corrections up to 20%–25% for  $Ra = 10^6$ ; for increasing Rayleigh numbers the correction decreases and, even if its magnitude depends on the aspect ratio of the cell and on the thermal properties of working fluid and side wall, it generally becomes negligible for  $Ra > 10^{11}$ . We will show that when the side wall correction ceases to be important the thermal resistance of the plates starts to affect the heat transfer. Unfortunately, in contrast to the side wall effect, the plate correction becomes more important as the Rayleigh number increases, it is essentially independent of the cell aspect ratio, and eventually it becomes the bottleneck of the system.

In order to further support the last statement we can resort to the following simple argument: even if it is now clear that a single power law does not fit the Nusselt vs Rayleigh curve<sup>9-12</sup> for our purposes we can still write  $Nu = a Ra^\beta$  (possibly with  $\beta$  function of  $Ra$ ) since we only need to note that  $Nu$  is a monotonically increasing function of  $Ra$ . From the definitions (1), the circuit in Fig. 1, the relations  $\Delta_i = R_i \dot{Q}_i$  and the correlation  $Nu = a Ra^\beta$  it is easy to show that the results

$$\Delta_T = \left[ 2R_p + \frac{AR_{sw}}{A + R_{sw}\Delta^\beta} \right] \dot{Q}, \quad (2)$$

with  $2R_p = R_{pl} + R_{pu}$  and  $A = h / (\lambda_f S a) [(v_f k_f) / (g \alpha_f h^3)]^\beta$ . Being  $\Delta_T = \Delta + 2R_p \dot{Q}$  for increasing  $\Delta_T$  also  $\Delta$  will grow and, if  $R_p$  and  $R_{sw}$  remain constant with  $\Delta_T$ , as  $\Delta_T \rightarrow \infty$  Eq. (2) reduces to  $\Delta_T = R_p \dot{Q}$ . This implies that regardless of how small  $R_p$  is, eventually it will dominate the thermal resistance of the whole setup.

Another point to be addressed is the temperature distribution on the plate surface for a finite value of the plate thermal conductivity. According to Schlichting<sup>13</sup> (p. 507) when a flow sweeps a solid surface the wall temperature can be considered constant provided the product  $A_w = \rho_w C_w \lambda_w$  is much larger than the analogous quantity  $A = \rho_f C_{pf} \lambda_f$  for the fluid: here  $\rho_w$ ,  $C_w$ , and  $\lambda_w$  are, respectively, the density, specific heat, and thermal conductivity of the material of the plate. As previously mentioned, in convective turbulence experiments the thermal plates are made by solid copper and in the best conditions, using the data for oxygen-free pure copper and gaseous helium a  $T \approx 5$  K, we have a ratio  $A_w/A \approx 31\,000$  (Ref. 14) which appears large enough to safely consider the plate surface isothermal. It must be stressed, however, that  $\lambda_f$  is only the molecular thermal conductivity of the fluid while, due to convection, what the plate surface "sees" is a fluid whose effective thermal conductivity is  $\lambda_{eff} = Nu \lambda_f$ . This implies that the ratio  $A_w/A_{eff}$  does not re-

main much larger than one for every value of the Nusselt number; in particular, using the previous values we find  $A_w/A_{\text{eff}}=1$  for  $\text{Nu}=31\,000$  which is obtained for Rayleigh numbers of the order of  $\text{Ra}\approx 10^{16}-10^{17}$  according to Ref. 4 or  $\text{Ra}\approx 10^{17}-10^{18}$  for Ref. 3. Such a large value of  $\text{Ra}$  has been approached by Ref. 3 and experimentalists are aiming at pushing the Rayleigh number further up. While for an order of magnitude argument it is sufficient to say that the value  $A_w/A_{\text{eff}}=1$  does not assure isothermal conditions at the plate/fluid interface, for the above extreme experimental conditions it is very important to determine a critical value of  $A_w/A_{\text{eff}}$  (or any related quantity) below which the thermal behavior of the plate is not adequate to the flow conditions.

To the author's knowledge only two papers have been devoted to study the finite conductivity effects of the plates on the dynamics of thermal convection, Refs. 7 and 15. The first paper tried to derive a model that, by accounting for the heat conductivity and heat capacity of the plates, could justify the differences among the existing experiments. In Ref. 15, on the other hand, a very detailed analysis of the effect of the plate properties on the generation and evolution of thermal plumes was performed. The aim of the present paper is to study by direct numerical simulations the influence of the plates thermal properties on the overall heat transfer (the Nusselt number) and to compute a correction factor that could be used by experimentalists to relate their measurements to the ideal flow free from finite conductivity effects.

We wish to stress that, although the analysis in this paper is limited to the "Rayleigh-Bénard" convection with constant temperature boundary conditions, the study of the effects of nonperfect thermal sources in turbulent convection is also relevant to the analysis of natural systems like the soil/atmosphere interaction or air/sea heat exchange where the two media have comparable thermal conductivities and heat capacities. In these cases, however, the thermal sources are only one of the parameters since heat radiation and interface topography play also a fundamental role.

## II. THE PROBLEM

### A. Numerical setup

We consider a fluid contained in a cylindrical cell of radius  $R$  and height  $h$  heated from below by a plate of thickness  $e$  with the lower horizontal surface maintained at constant temperature  $T_h$  (see Fig. 2). The fluid is cooled from above by an analogous plate of thickness  $e$  with the upper surface kept at temperature  $T_c$  with  $T_c < T_h$ . The thermal properties of the plates are different from those of the fluid and denoted by the subscript  $w$ . The lateral wall is perfectly adiabatic and all the wetted surfaces are all no-slip. The flow investigated in this paper is that developing in the cylindrical cell of aspect ratio  $\Gamma = 2R/h = 1/2$ .

The purpose of the setup sketched in Fig. 2 is to mimic the flow conditions of an experiment in which the horizontal plates exhibit their own heat transfer dynamics and this interacts with the heat transfer in the fluid.

We wish to stress that the boundary condition of uniform constant temperature on one side of the plates is equivalent to consider the presence of infinite heat capacity devices at

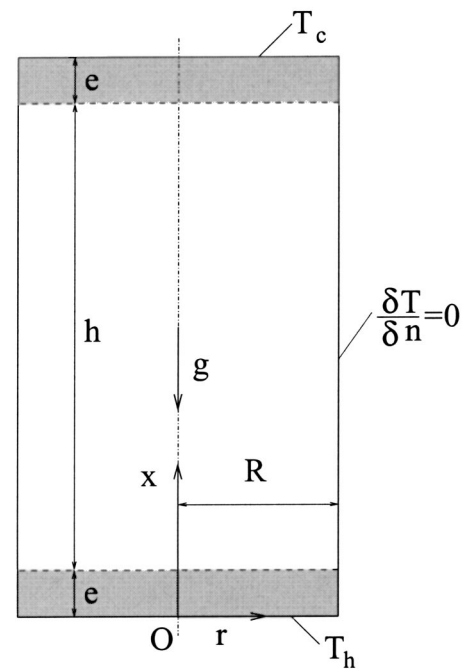


FIG. 2. Sketch of the cell.

the two extremes of the computational setup. These conditions are only approximately true in a laboratory experiment where the plates are heated and cooled using different techniques and implying different constructive details (thickness and geometry). Cioni, Ciliberto and Sommeria,<sup>16</sup> for example, in their cell with mercury showed that the dynamics of the hot plate is better described by a constant heat flux boundary condition while the cold plate can indeed be considered a constant temperature surface. It is worth mentioning that the particular behavior of the plate and fluid depends on their nature and also on the Rayleigh number; nevertheless the difference of temperature boundary conditions between numerical simulations and experiments must be kept in mind when considering the effect of the plate thickness on the heat transfer (see Sec. III D).

The flow evolution was simulated by numerically integrating the Navier-Stokes equations with the Boussinesq approximation in the case of variable thermal properties of the medium. If  $V_f$  is the fluid domain ( $e \leq x \leq h + e$ ,  $0 \leq r \leq R$ , and  $0 \leq \phi < 2\pi$  with  $\phi$  the azimuthal coordinate) and  $V$  is the total domain, the nondimensional governing equations are

$$\frac{D\mathbf{u}}{Dt} = -\nabla p + \theta \hat{x} + \left(\frac{\text{Pr}}{\text{Ra}}\right)^{1/2} \nabla^2 \mathbf{u}, \quad \nabla \cdot \mathbf{u} = 0, \quad \text{on } V_f, \quad (3)$$

$$\frac{D\theta}{Dt} = \frac{1}{(\text{Pr Ra})^{1/2}} \frac{\rho_f C_{pf}}{\rho C} \nabla \cdot \left( \frac{\lambda}{\lambda_f} \nabla \theta \right), \quad \text{on } V, \quad (4)$$

being  $\rho$ ,  $C$ , and  $\lambda$  the quantities for the fluid ( $\rho_f$ ,  $C_{pf}$ , and  $\lambda_f$ ) or the solid ( $\rho_w$ ,  $C_w$ , and  $\lambda_w$ ) depending on the position in the domain  $V$ .

$\hat{x}$  is the unity vector pointing in the opposite direction with respect to gravity,  $\mathbf{u}$  the velocity vector,  $p$  the pressure (separated from its hydrostatic contribution), and  $\theta$  the non-

dimensional temperature. The equations have been made nondimensional using the free-fall velocity  $U = \sqrt{g\alpha_f\Delta_T h}$ , the height of the fluid layer  $h$  and the maximum temperature difference  $\Delta_T = T_h - T_c$ ; the nondimensional temperature  $\theta$  is defined  $\theta = (T - T_c)/\Delta_T$  so that  $0 \leq \theta \leq 1$ . Pr is the Prandtl number defined as  $\text{Pr} = \nu_f/k_f$ .

The numerical method is that described in Ref. 17 with the implementation of an immersed boundary procedure<sup>18</sup> allowing the solution of the momentum and temperature equations on different domains. The validation of the whole code against experimental and analytical results is given in Refs. 11 and 19. Here only a brief description of the method is given. The equations have been written in cylindrical coordinates and discretized on a staggered mesh by central second-order accurate finite-difference approximations; the resulting discretized system is solved by a fractional-step procedure with the elliptic equation inverted using trigonometric expansions in the azimuthal direction and the FISHPACK package<sup>20</sup> for the other two directions. The time advancement of the solution is obtained by a hybrid low-storage third-order Runge–Kutta scheme.

## B. Simulation plans

It is now well documented in the literature that the most important parameters in turbulent thermal convection are the Rayleigh and Prandtl numbers. The aspect ratio of the cell  $\Gamma$  (Ref. 1) and even the cell shape<sup>21</sup> have also an influence on the flow dynamics, especially in slender cells. Looking at Eqs. (3) and (4) and at the sketch of Fig. 2 additional parameters must be considered, namely the ratios  $D = (\rho_f C_{pf})/(\rho_w C_w)$  and  $\lambda_w/\lambda_f$  and the relative plate thickness  $e/h$ . Considering that each set of flow parameters implies a three-dimensional direct numerical simulation of Eqs. (3) and (4), it is clear that the complete analysis of a flow depending on six independent variables is not within the reach of a single research project.

In order to reduce the computational effort, two main strategies have been followed: we have identified a particular cell geometry and working fluid in such a way to fix  $\Gamma$  and Pr. Since the experiments in which the highest values of Rayleigh have been attained are those reported in Refs. 3 and 4 that used gaseous helium in a slender cylindrical cell, we have posed  $\Gamma = 1/2$  and  $\text{Pr} = 0.7$ . Within this setup we have made extensive use of axisymmetric numerical simulations to span a wide range of the remaining parameters and to figure out their effects on the heat transfer. We have thus performed three-dimensional numerical simulations only to check that the findings conjectured from axisymmetric flows could be extended to full three-dimensional flows.

An additional advantage of using the setup with  $\Gamma = 1/2$  and  $\text{Pr} = 0.7$  is that being the physical problem (and the structure of the numerical code) essentially the same as that of Refs. 11 and 19 we could use those simulations to assess the resolution requirements and to validate the numerical procedure. In particular grids from  $33 \times 49 \times 97$  up to  $129 \times 65 \times 301$  nodes, respectively in the azimuthal, radial and vertical directions have been used for Ra in the range  $2 \times 10^6 - 2 \times 10^9$ ; this ensures the mesh size to be of the order

of the Kolmogorov scale in the bulk of the flow and the viscous and thermal boundary layers to be adequately resolved.<sup>19</sup>

In the axisymmetric cases only a meridional  $r-x$  plane was solved and neither the spatial resolution, nor the CPU time was a limiting factor. As a result simulations on  $49 \times 97$  up to  $193 \times 785$  points have been run for  $10^6 \leq \text{Ra} \leq 10^{10}$  and grid refinement checks were performed concerning the solution sensitivity to Ra,  $D$ , and  $\lambda_w/\lambda_f$ .

## C. Axisymmetric vs three-dimensional simulations

We wish to stress that, although we will make intensive use of axisymmetric simulations, their Nusselt vs Rayleigh relation is different with respect to the three-dimensional case;<sup>22</sup> this implies that every result conjectured from axisymmetric flows can not be extended to three-dimensional configurations without a cross check with the appropriate simulation.

The main differences between the two flows are due to the different plume dynamics and to the mean flow structure: in fact, depending on the initial perturbations it is possible to force the axisymmetric mean flow in two different stable configurations, the first with an uprising central plume and the second with a descending one (see Fig. 3). In both cases the Nusselt number attains the same value [ $\text{Nu} = 39.5 \pm 2.2$  in the first and  $\text{Nu} = 39.0 \pm 2.1$  in the second at  $\text{Ra} = 2 \times 10^8$ ,  $e/h = 0.05$ ,  $\lambda_f/\lambda_w = 50$ , and  $D = \rho_f C_{pf}/(\rho_w C_w) = 1$ ], and the only noticeable difference is the mean flow temperature which, respectively, oscillates below and above the mean plates temperature  $\theta = 0.5$ . This result confirms the theoretical prediction by Ref. 23 and it is a peculiarity of the axisymmetric flow; in the three-dimensional flow, in fact, the large scale structures are not axisymmetric and any deviation of the mean flow temperature  $\theta = 0.5$  disappears.

As an example a snapshot of a vertical section of a three-dimensional flow is reported in Fig. 4(a) showing the very different flow organization with respect to the axisymmetric flow. This difference is further confirmed by the mean cell temperature of Fig. 4(b) always oscillating about the mean value  $\theta = 0.5$  in contrast to Fig. 3(c).

## III. RESULTS

### A. Effects on a single plume

In this section we show the effect of the finite thermal conductivity of the lower hot plate on the dynamics of a single plume. The reason for performing this preliminary analysis is that thermal plumes are responsible for most of the heat transfer in the cell (at least for  $\text{Pr} \geq 0.3$  as indicated by Ref. 24) and from the observed changes in the plume behavior some consequences on the complete flow can be conjectured. A thermal plume can be thought of as a portion of fluid elongated in the vertical direction whose temperature is hotter (if ascending) or colder (if descending) than the ambient fluid; since in these structures temperature and vertical velocity are generally highly correlated, plumes act as driving engines for the heat transfer.

In Fig. 5 the time evolution of an axisymmetric plume

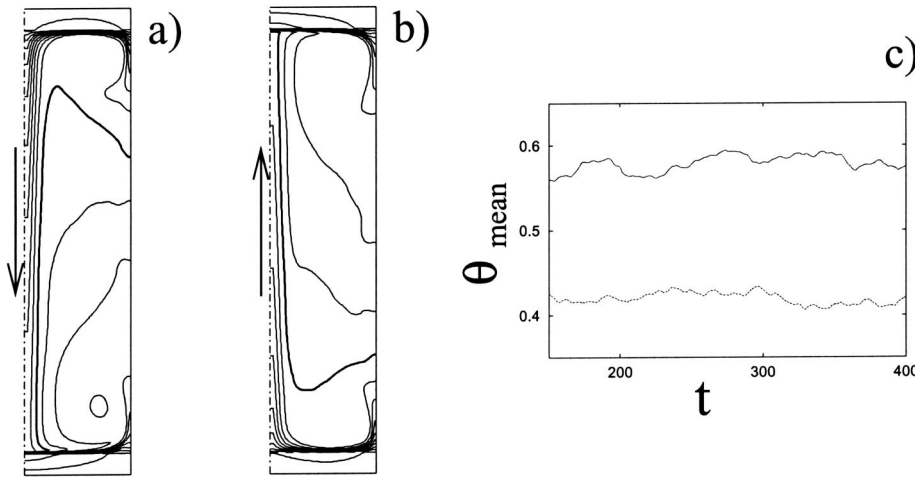


FIG. 3. Time averaged temperature contours ( $\Delta\theta=0.05$ ) for axisymmetric flows at  $Ra=2\times 10^8$ ,  $e/h=0.05$ ,  $\lambda_f/\lambda_w=50$ , and  $D=1$ . (a) Descending plume, (b) uprising plume; the thick solid line is  $\theta=0.5$ . (c) Time evolution of the volume averaged temperatures. —, Descending plume; ---, uprising plume.

detaching from the lower hot plate is shown for three different values of the plate thermal conductivity. In particular, at  $t=0$  the initial temperature field inside the plate is given by the steady purely conductive solution while the fluid temperature is set everywhere at  $\bar{\theta}=0.5$  except within a layer in contact with the plate whose thickness is adjusted to that of the thermal boundary layer at the imposed Rayleigh number [ $\delta_\theta/h \approx 1/(2Nu)$ ,  $Nu$  is taken from an axisymmetric simulation of the complete flow]. An additional radial perturbation is assigned in order to fix the plume detachment in the region around the symmetry axis, therefore the initial temperature field reads

$$\theta(r,x) = 1 - \frac{\lambda_w x}{\lambda_f}, \quad \text{for } r \geq 0, \quad 0 \leq x \leq e, \tag{5}$$

$$\theta(r,x) = \bar{\theta} + \left(1 - \frac{\lambda_w e}{\lambda_f} - \bar{\theta}\right) e^{[r/\delta_\theta]^2} e^{[(x-e)/\delta_\theta]^2},$$

for  $r \geq 0, \quad x \geq e$ .

Simulations for three different values of  $\lambda_w/\lambda_f$  have been performed and the results of Fig. 5 show that already at  $t=1$

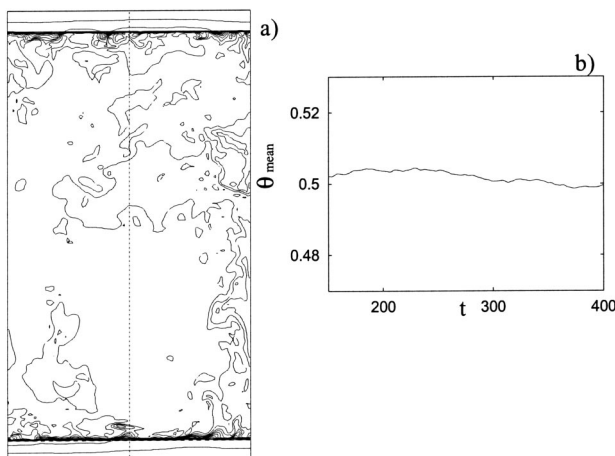


FIG. 4. (a) Snapshot of temperature contours in a vertical section through the axis.  $Ra=2\times 10^9$ ,  $D=1$ ,  $\lambda_w/\lambda_f=50$ ,  $e/h=0.05$ ,  $\Delta\theta=0.04$ . (b) Time evolution of the volume averaged temperature for the flow in (a).

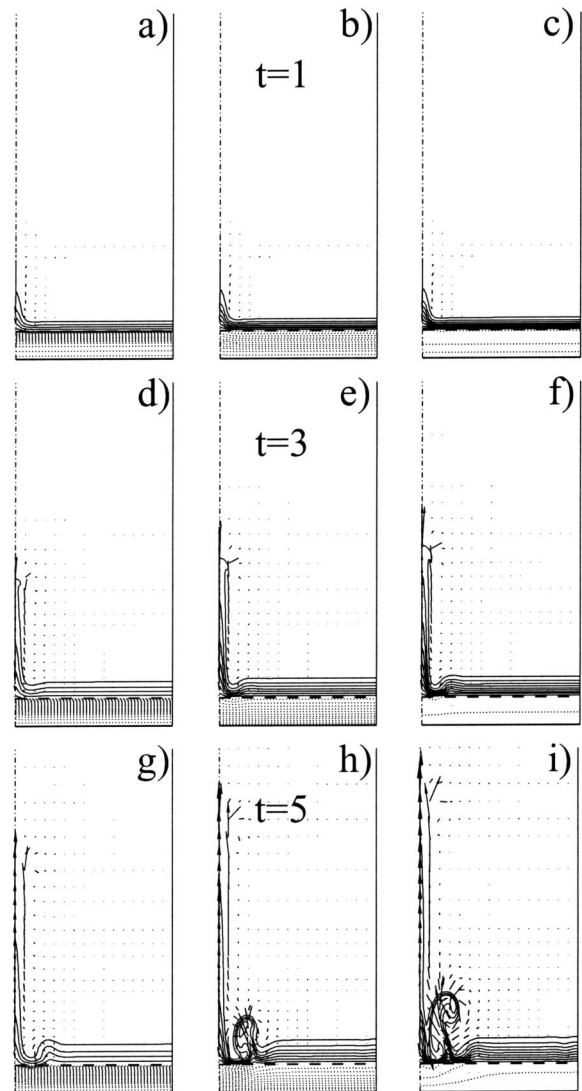


FIG. 5. Time evolution of an axisymmetric single thermal plume at  $Ra=2\times 10^9$ ,  $Pr=0.7$ ,  $e/h=0.05$ , and  $D=1$ . Panels (a), (d), and (g) are at  $\lambda_w/\lambda_f=1$ ; (b), (e), and (h) at  $\lambda_w/\lambda_f=10$ ; (c), (f), and (i) at  $\lambda_w/\lambda_f=100$ . —, Temperature contour lines in the fluid ( $\Delta\theta=0.05$ ); ···, temperature contour lines in the hot plate ( $\Delta\theta=0.01$ ). Velocity vectors are overlaid on the temperature contours.

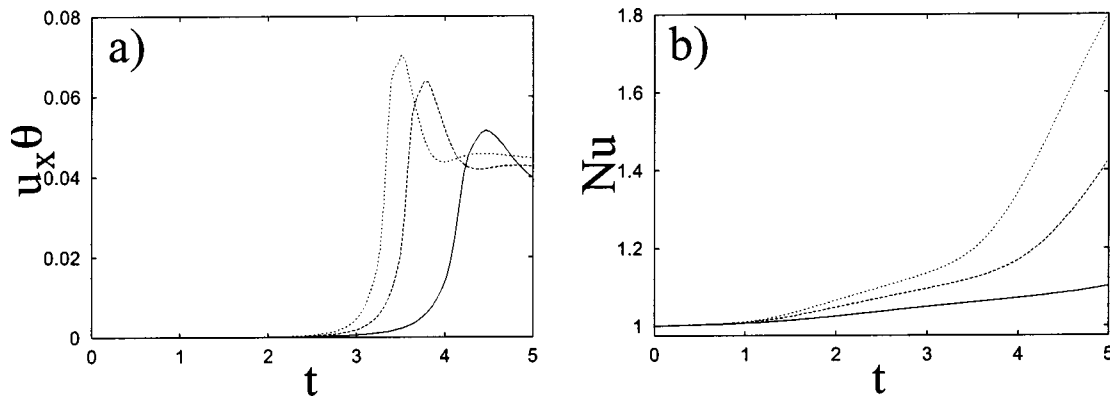


FIG. 6. (a) Time evolution of the product  $u_x \theta$  in the point on the symmetry axis at a distance  $x/h=0.25$ . (b) Time evolution of the Nusselt number. —,  $\lambda_w/\lambda_f=1$ ; ---,  $\lambda_w/\lambda_f=10$ ; ···,  $\lambda_w/\lambda_f=100$ .

the fluid around the axis of symmetry moves upward while other fluid moves radially inward and sweeps the hot plate. The uprising plume increases its velocity according to the temperature difference with the ambient fluid, the former, in turn, depending on the heat the plate has transferred to the plume. In this scenario it might be possible that the plate is not fast enough to provide the heat requested by the plume thus stopping its growth and preventing further fluid from being heated. This is exactly the phenomenon observed in Fig. 5, where it can be noted that, depending on the ratio  $\lambda_w/\lambda_f$ , not only the evolution of the primary plume is delayed but also the formation of those structures, forming at the plate surface after the plume detachment. More quantitative information is given in Fig. 6 showing for the flows of Fig. 5 the time evolution of the convective heat transport and the Nusselt number; in particular, Fig. 6(a) shows that the smaller the ratio  $\lambda_w/\lambda_f$  the less heat is convected by the primary plume and this is reflected also by the global heat transport [Fig. 6(b)].

The same phenomena are observed in a full three-dimensional configuration as shown in Fig. 7, where an instantaneous snapshot of the velocity vectors in a vertical plane cut and the temperature distribution at the fluid/plate interface are reported. In particular it can be seen that where a vertical descending cold current sweeps the plate surface the temperature locally decreases below the mean value; as the fluid moves parallel to the plate it gradually warms up and the local plate temperature also increases. At the end of the plate the fluid gains enough heat to detach from the wall and to generate a new rising current.

The dynamics of the plume formation and development as function of the thermal properties of the hot plate have been investigated in detail by Ref. 15. The present findings can be therefore interpreted in view of those results: their main conclusion is that if the thermal diffusivity of the plate  $k_w$  is much larger than that of the fluid  $k_f$  than regular plumes develop and they can extend to the top of the fluid layer. When the plate diffusivity is low, in contrast ( $k_w \ll k_f$ ) the surface cools below the developing plume and it either breaks up into puffs or puffs are generated directly near the surface. Of course, in thermal convection laboratory experiments, it never happens that  $k_w$  is of the same order as

$k_f$ , nevertheless considering that the plate transfers the heat to a material whose effective thermal diffusivity is  $k_{\text{eff}} = \text{Nu} k_f$ , then they become comparable if the Rayleigh number is high enough.

An alternative way of looking at the plate effects on the plume dynamics is by the following dimensional argument: according to the picture given by Ref. 25 the time interval between two successive emissions of thermal plumes from the plate is on the average  $\tau_p^* \approx \delta_0^2/k_f$  which can be written in the nondimensional form  $\tau_p \approx (\text{Ra Pr})^{1/2}/(4 \text{Nu}^2)$ . On the other hand, once a plume has detached new fluid from the bulk at temperature  $\theta \approx 0.5$  comes in contact with the plate and it needs to be heated before a new plume can be released. The fresh fluid, on the other hand, cools the plate surface and if the latter does not provide enough heat the plume formation can be slowed down or even stopped. A rough way to estimate the time scale for the plate is by evaluating its diffusive time  $\tau_p^* \approx e^2/k_w$  which can be rewritten in nondimensional form  $\tau_p \approx (\text{Ra Pr})^{1/2}(e/h)^2(k_f/k_w)$ . This simplified picture already points out the essence of the

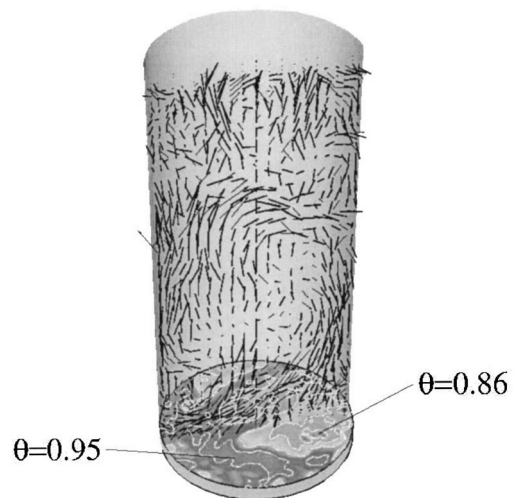


FIG. 7. Instantaneous snapshot of velocity vectors in a vertical plane through the symmetry axis and contour levels of temperature at the lower plate/fluid interface:  $\text{Ra}=2 \times 10^9$ ,  $(\rho C_p)_f/(\rho C_p)=1$ ,  $\lambda_w/\lambda_f=50$ ,  $e/h=0.05$ ,  $\Delta\theta=0.01$ .

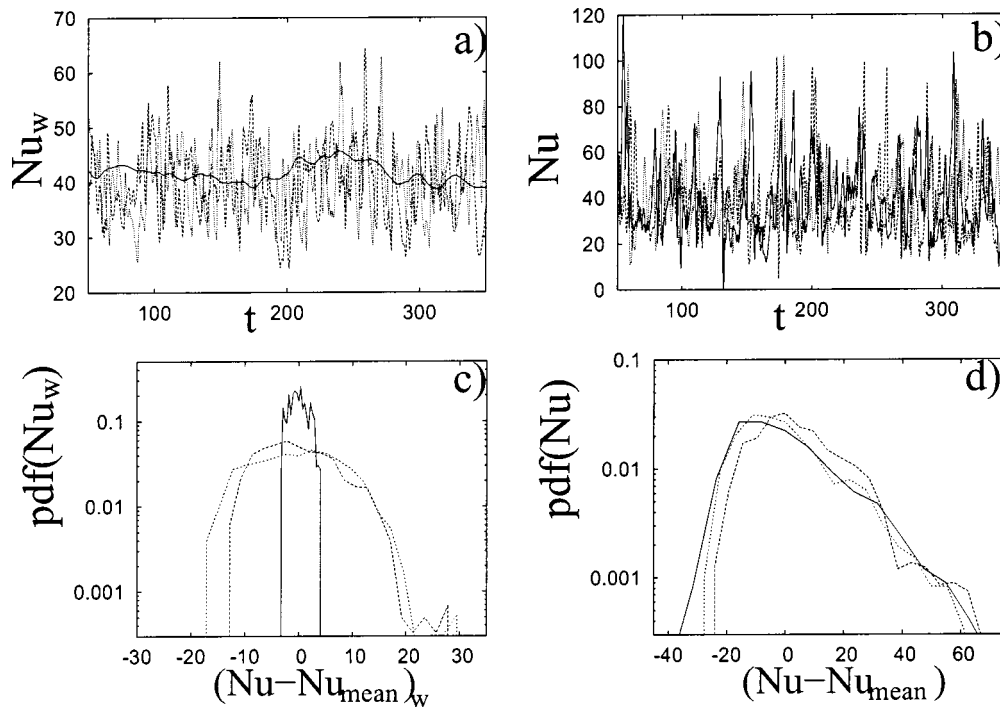


FIG. 8. (a) Time evolution of the Nusselt number evaluated as surface integral over the lower hot plate at  $Ra=2 \times 10^8$ ,  $e/h=0.05$ , and  $\lambda_w/\lambda_f=50$ . —,  $D=0.01$ ; ---,  $D=1$ ;  $\cdots$ ,  $D=100$ . (b) The same as (a) but for the Nusselt number evaluated as volume integral. (c) and (d) are the histograms, respectively, of the curves in panels (a) and (b).

problem since  $\tau_p$  increases with  $Ra$  while  $\tau_f$  decreases (at least if in the power law  $Nu \sim Ra^\beta$  it is  $\beta > 1/4$ ). If the dynamics of the heat transfer in the plate does not have to interfere with the dynamics of the fluid it should be  $\tau_p/\tau_f \ll 1$ , while on the other hand, we have  $\tau_p/\tau_f \approx 4 Nu^2 (e/h)^2 (\lambda_f/\lambda_w)/D$  which, regardless of the plate geometry and material properties, cannot asymptotically satisfy the condition  $\tau_p/\tau_f \ll 1$ . In the next sections we will investigate the dependence of the Nusselt number on each parameter separately with the aim of identifying the most important effects and deriving a correction factor for the  $Nu$  vs  $Ra$  relationship.

A variation to the above behavior is given by the experiment with cryogenic helium by Ref. 3; in fact in that case the Rayleigh number is varied by approaching the helium critical point and the divergence of the constant pressure specific heat  $C_p$  brings to  $k_f \sim Ra^{-1/2}$ .<sup>26</sup> In other words, the experiments are performed as if a continuous range of different fluids were available and this yields the peculiar behavior of  $k_f$ . Nevertheless, even if in that cryogenic helium experiment it results  $k_f \sim Ra^{-1/2}$ , also in that case the ratio  $\tau_p/\tau_f$  increases with  $Ra$ , although at a slower rate than in standard experiments. This happens because in the correlation  $Nu \sim Ra^\beta$  it is  $\beta > 1/4$  and the ratio  $\tau_p/\tau_f$  increases as  $Nu^2$ . On the other hand, in the experiments by Refs. 4 and 27 the plates temperature difference could be varied continuously and  $k_f$  resulted independent of  $Ra$ ; these experiments, therefore, behave in the same way as standard experiments with noncryogenic fluids.

## B. Dependence on $D$

According to the previous section, one of the parameters influencing the heat transfer might be  $D = (\rho_f C_{pf})/(\rho_w C_w)$ , the ratio of the heat capacity per unit volume of fluid and plates. It is important to note that, depending on the material of the plates and the particular fluid,  $D$  can span a wide range of values; for example, for oxygen free copper and helium at  $T \approx 5$  K we have  $D=3.58$ , for copper and air at ambient temperature it results  $D=4.5 \times 10^{-4}$  while for brass and water we have  $D=1.26$ . We have performed axisymmetric simulations for several values of  $Ra$  ( $2 \times 10^6$ ,  $2 \times 10^8$ , and  $2 \times 10^{10}$ ), and  $\lambda_f/\lambda_w$  (50 and 200) with  $D$  in the range  $10^{-2} \leq D \leq 10^2$ , always observing a negligible dependence of the mean Nusselt number on  $D$ . The Nusselt number can be evaluated by computing directly the mean heat flux at the hot and cold plates  $Nu_w = \partial\theta/\partial x|_w$  (where  $|_w$  indicates that the derivative is evaluated at the wall and the overbar implies an average in time and over the plate surface) or, resorting to the conductive and convective heat transfer definitions, by  $Nu = 1 + \sqrt{Ra Pr} \langle u_x \theta \rangle$  (with the angular brackets indicating average over time and over the whole fluid layer). Although, on the average, the two definitions converge to the same value, the former accounts for the dynamics within the thermal boundary layer while the latter stresses the motion in the bulk of the flow. Typical results are reported in Fig. 8 showing for the same flows the time evolution of  $Nu$  computed in different ways. In Fig. 8(a) we see that the lower the value of  $D$  the smaller are the fluctuations of the Nusselt number about the average; the fluctuations in Fig. 8(b), in contrast,

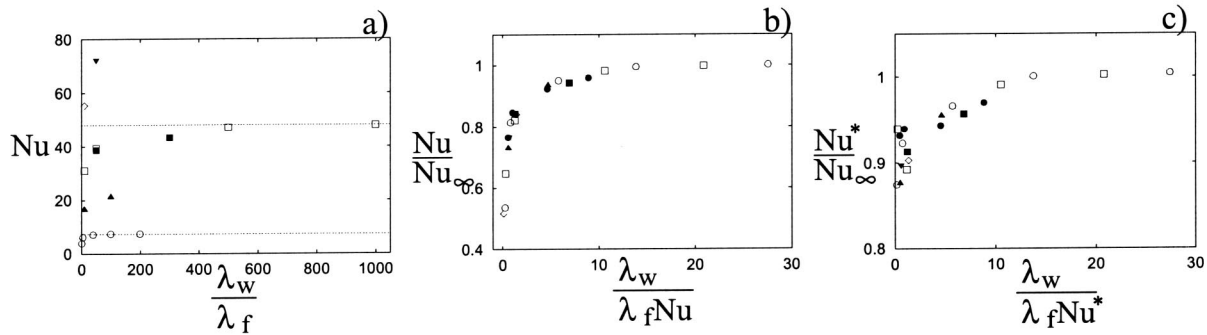


FIG. 9. (a)  $Nu$  vs  $\lambda_w/\lambda_f$  for different Rayleigh numbers at  $D=1$  and  $e/h=0.05$ . — and --- are, respectively, the  $Nu_\infty$  values for the axisymmetric flows at  $Ra=2\times 10^6$  and  $Ra=2\times 10^8$ . (b) The same as (a) but for  $Nu/Nu_\infty$  vs  $\lambda_w/(Nu\lambda_f)$ .  $\circ$ , Axisymmetric  $Ra=2\times 10^6$ ;  $\bullet$ , three-dimensional  $Ra=2\times 10^6$ ;  $\triangle$ , axisymmetric  $Ra=2\times 10^7$ ; solid  $\triangle$ , three-dimensional  $Ra=2\times 10^7$ ;  $\square$ , axisymmetric  $Ra=2\times 10^8$ ;  $\blacksquare$ , three-dimensional  $Ra=2\times 10^8$ ;  $\nabla$ , axisymmetric  $Ra=2\times 10^9$ ; solid  $\nabla$ , three-dimensional  $Ra=2\times 10^9$ ;  $\diamond$ , axisymmetric  $Ra=2\times 10^{10}$ . (c) The same as (b) but using  $Nu^*$  instead of  $Nu$ .

are essentially independent of  $D$ . The reason is that in the first case the heat stored in the plate can level out the peaks of temperature gradients between plate and fluid and this mechanism is enhanced by the increased heat capacity of the plate. The bulk definition of the Nusselt number, on the other hand, is mediated by the mean temperature of the fluid which is more related to the dynamics of the large-scale structures. The same information is given by Figs. 8(c)–8(d) showing, respectively, the histograms for the curves in Figs. 8(a) and 8(b). Considering the average  $Nu$  of Fig. 8 we find  $Nu=39.1\pm 2.1$ ,  $Nu=39.7\pm 2.2$  and  $40.2\pm 1.2$ , respectively, for  $D=100$ ,  $D=1$ , and  $D=0.01$ ; even if it is tempting to conjecture a weak  $Nu$  increase with decreasing  $D$  (and this would be consistent with the plume dynamics shown in the previous section) we can conclude that the Nusselt variations are within the error bars and these are negligible when compared to the changes induced by other factors. The very limited sensitivity of  $Nu$  on  $D$  is mainly a consequence of the steady temperature boundary conditions of the setup, since the product  $\rho_w C_w$  affects the relaxation time of the plates when switching from one state to another. On the other hand, each plate has one surface maintained at a fixed temperature and the other surface (the wetted one) whose temperature is statistically steady owing to the large number of random events occurring on the fluid side. In other words, if the mean plates temperature were time dependent, then the thermal diffusivity (or  $D$ ) would be a decisive factor. In contrast, being the mean plate temperature statistically steady, the thermal diffusivity plays a minor role with respect to other factors. Further details on temperature fluctuations inside the plate and the steadiness of the temperature profile are given in Appendix A for a simplified model problem.

### C. Dependence on $\lambda_w/\lambda_f$

As we have seen in Sec. III A the generation and evolution of thermal plumes is strongly influenced by the ratio of the thermal conductivities of fluid and plate. In fact, since  $\lambda_w$  remains constant with  $Ra$  while the effective conductivity of the fluid increases with  $Ra$  according to  $\lambda_{\text{eff}}=Nu\lambda_f$ , eventually the thermal conductivity of the plate becomes too small to allow the requested heat flux. The same mechanism governs the whole flow and typical results are given in Fig.

9(a) showing the  $Nu$  vs  $\lambda_w/\lambda_f$  curves for different values of  $Ra$ . When  $\lambda_w/\lambda_f$  exceeds a threshold (whose value is  $Ra$ -dependent) the Nusselt number becomes essentially independent of  $\lambda_w/\lambda_f$  and converges to the asymptotic value  $Nu_\infty$  obtained when the temperature boundary conditions are imposed directly at the plate/fluid interface.<sup>19</sup>

The conjecture that the plates “see” a material with effective thermal conductivity  $Nu\lambda_f$  is confirmed by Fig. 9(b) in which all the results for different values of  $Ra$  and  $\lambda_w/\lambda_f$  collapse onto a single line when the quantities  $Nu/Nu_\infty$  vs  $\lambda_w/(Nu\lambda_f)$  are plotted. We wish to stress that in Fig. 9(b) we have on the same curve three-dimensional and axisymmetric simulations despite the very different mean flow structure and plume dynamics.

It is worth noting that the unique collapse of axisymmetric and three-dimensional results of Fig. 9(b) does not imply neither the same values of the Nusselt number nor the same scaling with  $Ra$  (see Ref. 22); the reason for the collapse is the presence in the abscissa of  $Nu$  which incorporates all the flow differences between axisymmetric and three-dimensional flows. Nevertheless the possibility of describing with a single relation both kinds of flow evidences the robustness of the scaling arguments and confirms the possibility of scanning the parameters range using fast axisymmetric simulation and of confirming the conjectures by fewer three-dimensional simulations.

Looking at Fig. 5 it is evident that part of the total temperature difference  $\Delta_T$  drops within the plates thickness thus implying that the effective temperature difference across the fluid layer is  $\Delta < \Delta_T$ . The Nusselt and Rayleigh numbers defined in the relations (1) can be therefore reformulated using  $\Delta$  instead of  $\Delta_T$  yielding

$$Nu^* = \frac{\dot{Q}h}{\lambda_f \Delta S} \quad \text{and} \quad Ra^* = \frac{g\alpha_f \Delta h^3}{\nu_f k_f}. \quad (6)$$

These quantities are more appropriate to those flows where either  $\Delta_T$  is corrected by the static conductive plates drop or when  $\Delta$  is measured directly by placing probes at the fluid/plate interfaces. In Fig. 9(c),  $Nu^*$  is used instead of  $Nu$  for the same plot as Fig. 9(b). We wish to stress that the difference between  $Nu^*$  and  $Nu_\infty$  is due only to the modified plume dynamics caused by the finite conductivity of the

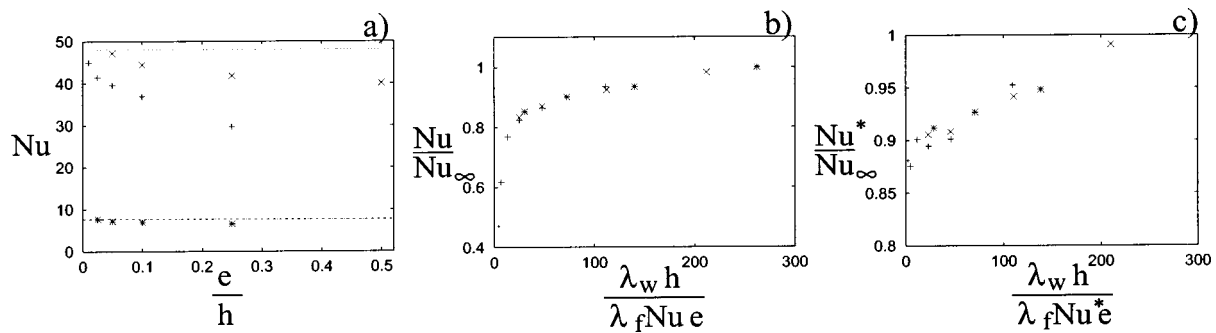


FIG. 10. (a) Nu vs  $e/h$  for different Ra and  $\lambda_w/\lambda_f$  at  $D=1$ . — and --- are, respectively, the  $Nu_\infty$  values for the axisymmetric flows at  $Ra=2 \times 10^6$  and  $Ra=2 \times 10^8$ . (b) The same as (a) but for  $Nu/Nu_\infty$  vs  $\lambda_w h / (\lambda_f Nu e)$ . \*, Axisymmetric  $Ra=2 \times 10^6$  and  $\lambda_w/\lambda_f=50$ ; +, axisymmetric  $Ra=2 \times 10^8$  and  $\lambda_w/\lambda_f=50$ ; x, axisymmetric  $Ra=2 \times 10^8$  and  $\lambda_w/\lambda_f=500$ ; +, axisymmetric  $Ra=2 \times 10^{10}$   $\lambda_w/\lambda_f=50$ . (c) The same as (b) but using  $Nu^*$  instead of Nu.

plates while the difference between Nu and  $Nu_\infty$  includes also the static effect of the reduced temperature difference.

A relevant observation in Figs. 9(b)–9(c) is that the deviation of the results from  $Nu/Nu_\infty=1$  is still appreciable at  $\lambda_w/(\text{Nu} \lambda_f)=10$  confirming the presence of finite conductivity effects even when the plate conductivity is one order of magnitude larger than the fluid effective conductivity. In addition, being the fluid effective conductivity dependent on Nu the argument  $\lambda_w/\lambda_f \gg 1$  should not be used since, depending of the Rayleigh number of the flow, it could lead to serious errors [see Fig. 9(a)].

#### D. Dependence on $e/h$

The influence of the plate thickness  $e/h$  is investigated in this section by axisymmetric simulations performed for several values of Ra and  $\lambda_w/\lambda_f$ . Some results are given in Fig. 10(a) showing a Nu decrease for increasing  $e/h$  and, once more, the entity of the decrease depends on the Rayleigh number and the  $\lambda_w/\lambda_f$  ratio. Taking advantage of the results of the previous section, however, it is relatively easy to account for the effects of Ra and  $\lambda_w/\lambda_f$  and to define the quantities  $Nu/Nu_\infty$  and  $\lambda_w h / (\lambda_f Nu e)$  which rescale all the data on a single curve [Fig. 10(b)]. It can be noted from Fig. 10(b) that for decreasing plate thicknesses ( $e \rightarrow 0$ ) we have  $Nu \rightarrow Nu_\infty$  consistently with the observation that eventually the temperature boundary conditions are applied directly at the plate/fluid interface. On the other hand, for increasing plate thickness we have a decreasing  $Nu/Nu_\infty$ . Once again the same plot as Fig. 10(b) is reported in Fig. 10(c) using  $Nu^*$  instead of Nu with the aim of stressing the effect only on the plume dynamics rather than on the overall heat transfer.

The above results might appear counterintuitive since they seem to indicate for an experimental setup that the thinner are the plates the closer is Nu to  $Nu_\infty$ . This apparent inconsistency is due to the different temperature boundary conditions in experimental setups and in the present numerical simulations. In fact, the presence of constant temperature surfaces ( $x=0$  and  $x=h+2e$  in Fig. 2) implies the existence of infinite heat capacity devices with the plates placed in between these devices and the fluid layer. In contrast, in a laboratory experiment the heat current is the controlled quantity which is produced by spiraling coils via the Joule effect;

thick copper plates are then necessary between the coils and the fluid in order to homogenize the heat flux over the wetted surface and to have a heat capacity to cope with the most intense flow events.

In an experimental setup, therefore, thick metal plates are needed to approximate as close as possible the condition of uniform constant temperature at the plate/fluid interface. In the present numerical simulations, in contrast, the plates only act as parasite thermal resistances in between the fluid layer and ideal infinite heat capacity devices capable of maintaining a uniform and constant temperature independently of the required heat flux.

#### E. Discussion

The results of Fig. 10 allow us to consider the influence of all flow parameters on the heat transfer, therefore also the results of Fig. 9, when rescaled in the same way, should collapse on the same curve. Evidence of this is given in Fig. 11 where two additional cross-check three-dimensional simulations have been added. The reason for running further simulations is that in the analyses of the previous sections we have always maintained fixed one or more flow parameters, while now we would like to test the validity of the curve in Fig. 11 when every variable assumes a value different from that used for the curve determination. In particular, a first simulation at  $Ra=10^8$ ,  $e/h=0.08$ ,  $\lambda_w/\lambda_f=162.35$  and  $D=0.5$  and a second at  $Ra=10^7$ ,  $e/h=0.035$ ,  $\lambda_w/\lambda_f=216.66$  and  $D=3$  have been performed and the results are also reported in Fig. 11. We have obtained in the first case  $Nu=31.6 \pm 1.8$  and in the second  $Nu=17.7 \pm 1.0$  yielding, respectively,  $R_f/R_p = \lambda_w h / (\text{Nu} \lambda_f e) = 64.32$  and  $349.16$  with  $Nu/Nu_\infty=0.901$  and  $0.982$  (the values of  $Nu_\infty$  at  $Ra=10^7$  and  $Ra=10^8$  have been interpolated from Ref. 19). A further three-dimensional simulation with the same parameters as the first cross-check run ( $Ra=10^8$ ,  $e/h=0.08$ ,  $\lambda_w/\lambda_f=162.35$ ) except for  $D$  was performed; in particular in this simulation it was assumed  $D=20$  instead of  $D=0.5$  with the aim of checking whether  $k_w/k_f$  rather than  $\lambda_w/\lambda_f$  is the relevant parameter to compute the correction of Fig. 11. In the present case we have obtained  $Nu=32.5 \pm 1.9$  to be compared with the value  $Nu=31.6 \pm 1.8$  obtained for  $D=0.5$ . It should be noted that by increasing  $D$  by a factor 40 only an increase of Nu of the order of 3% was obtained. If the ther-

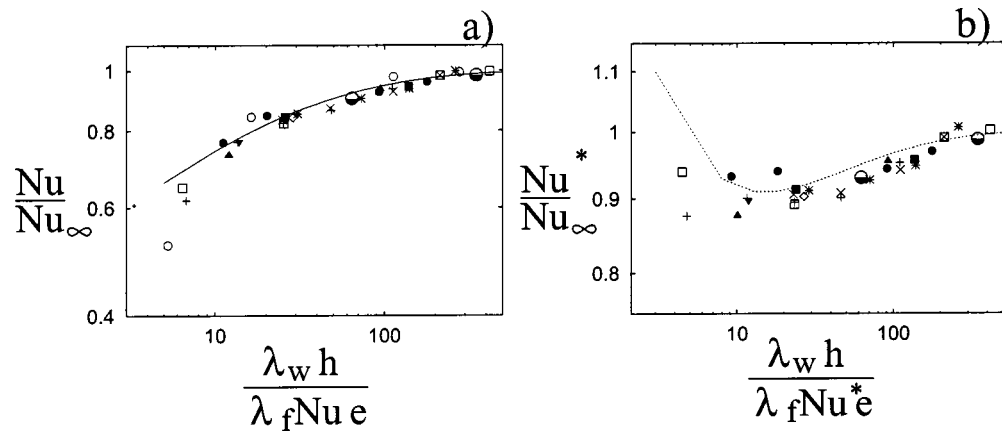


FIG. 11. (a)  $Nu/Nu_\infty$  vs  $\lambda_w h / (\lambda_f Nu e)$  for the results of Figs. 9 and 10 (with the same meaning of the symbols). Half-solid  $\circ$ , for cross-check three-dimensional simulations. —, Fit of the data:  $y = 1 - \exp[-(x/4)^{1/3}]$ . (b) The same as (a) but for  $Nu^*$  and  $Ra^*$  instead of  $Nu$  and  $Ra$ . ---, Ratio  $Nu^*/Nu_\infty (y = \{1 - \exp[-(x/4)^{1/3}]\} / (x - 2))$ .

mal diffusivities  $k_w$  and  $k_f$  had to be used in Fig. 11 instead of the thermal conductivities  $\lambda_w$  and  $\lambda_f$ , an increase of  $D$  by a factor 40 would have been equivalent to a decrease of  $\lambda_w/\lambda_f$  by the same factor. The latter would have given a value  $R_f/R_p = 1.6$  (instead of the original  $R_f/R_p = 64.32$ ) yielding a Nusselt number decrease of 47.5%; this is clearly not compatible with the result of the simulation which, in contrast, shows a small Nusselt number increase of magnitude smaller than the error bar. The fact that  $\lambda_w/\lambda_f$  is the relevant ratio and not  $k_w/k_f$  implies that the heat transfer inside the plates is essentially steady; in the Appendix a simplified one-dimensional unsteady problem for the heat transfer inside the plate is solved, and the results show that indeed when the plates correction becomes significant the temperature profile within most of the plate thickness is linear and steady. In contrast, the temperature unsteadiness induced by the flow dynamics at the upper surface only affects a very limited region of the plate adjacent to the plate/fluid interface.

Once we have verified that the appropriate scaling variables are  $\lambda_w h / (\lambda_f Nu e)$  and  $Nu/Nu_\infty$ , it is relatively easy to interpret this result in view of Fig. 1. In fact for the setup sketched in Fig. 2 it results in  $R_{sw} = 0$  and  $R_{up} = R_{lp} = R_p$ ; on the other hand the thermal analog of Ohm's law  $\Delta_i = R_i \dot{Q}_i$  requires  $R_p = e / (\lambda_w S)$  and  $R_f = h / (\lambda_{eff} S) = h / (\lambda_f Nu S)$ ,  $S$  being the wetted surface of the plate. It is then clear that the governing variable  $\lambda_w h / (\lambda_f Nu e)$  is just the ratio  $R_f/R_p$  and the condition  $Nu/Nu_\infty \approx 1$  is only obtained when  $R_f/R_p \gg 1$ ; the most important information of Fig. 11 is that we are now able to define a threshold value of  $R_f/R_p$  in order to neglect the finite conductivity effects of the plate. On the other hand, it must be noted that  $R_f/R_p = \lambda_w h / (\lambda_f Nu e)$  depends on the Nusselt number, therefore, for increasing  $Ra$ , regardless of the fluid and plate properties,  $R_f/R_p$  always becomes smaller than the fixed threshold.

It is worth mentioning that the Nusselt number of Fig. 11(a) is defined using the total temperature difference  $\Delta_T$  while in some experiments only the fluid temperature difference  $\Delta$  is used (see for example, Ref. 28) and it is estimated by subtracting the temperature drop within the plates  $\Delta_p$

(with  $\Delta = \Delta_T - \Delta_p$ ). In this case, being the temperature drop in the plates  $\Delta_p = 2R_p \dot{Q}$ , it is possible to write

$$Nu^* = \frac{\dot{Q}h}{\lambda_f \Delta} = Nu \frac{\Delta T}{\Delta} = Nu \frac{R_f/R_p}{R_f/R_p - 2} \quad (7)$$

and, since the relation between  $Nu$  and  $Nu_\infty$  is known from Fig. 11(a), it is possible to relate  $Nu^*$  with  $Nu_\infty$ .<sup>29</sup> The ratio  $Nu^*/Nu_\infty$  is reported in Fig. 11(b), where it is noted that it is practically coincident with  $Nu/Nu_\infty$  for  $R_f/R_p \geq 100$  when the difference becomes smaller than 2%; most of experiments are just in this range and the two corrections practically coincide. When the fluid is mercury, however,  $R_f/R_p$  is generally smaller than 100 and the difference between  $Nu^*$  and  $Nu$  becomes non-negligible. The community of experimentalists using mercury is apparently aware of this difference since in their plots  $Nu^*$  is always reported; in this case the difference between  $Nu^*$  and  $Nu_\infty$  is at most 11% for  $R_f/R_p \approx 11$  while the difference between  $Nu$  and  $Nu_\infty$  is already 25%. For smaller values of  $R_f/R_p$  the Nusselt number correction must be taken with caution since the empirical fit to  $Nu/Nu_\infty$  remains finite and, being the relation (7) between  $Nu^*$  and  $Nu$  exact,  $Nu^*/Nu_\infty$  estimated by the empirical fit yields, in the limit  $R_f/R_p \rightarrow 2$ ,  $Nu^*/Nu_\infty \sim (R_f/R_p - 2)^{-1}$  which is not physically realistic. One possible cause for this behavior is that for very small values of  $R_f/R_p$  most of the temperature drop occurs within the plates and the temperature difference in the fluid layer is so reduced that the developing flow can change in nature (unsteady laminar or even steady) with respect to the reference turbulent flow. This has been noticed, in particular, in those cases where small values of  $R_f/R_p (< 10)$  are combined with small values of Rayleigh numbers ( $Ra \leq 2 \times 10^7$ ). However it should be noted that the Nusselt number correction for  $R_f/R_p \rightarrow 0$  is only a speculative point since an underlying assumption of laboratory experiments is  $R_f/R_p \gg 1$  and in this limit  $Nu$  and  $Nu^*$  behave in a similar way. On the other hand it is worth mentioning that the fit of Fig. 11(a) is not accurate for  $R_f/R_p < 10$  since the numerical simulations seem to give values of  $Nu/Nu_\infty$  smaller than the curve and the divergence of  $Nu^*/Nu_\infty$  for

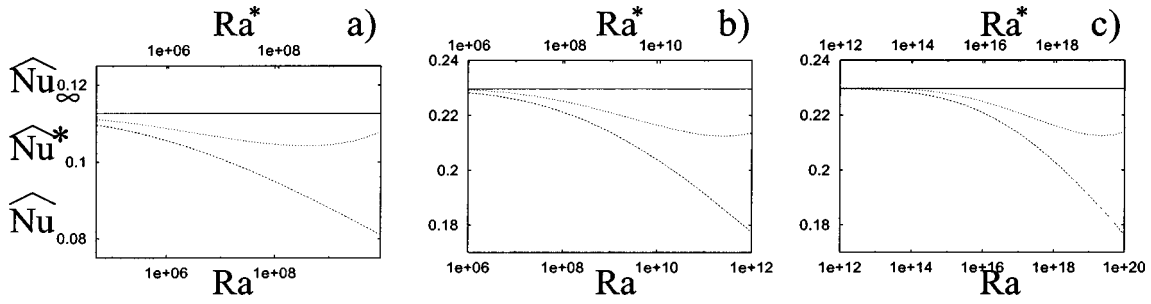


FIG. 12. Compensated Nusselt numbers for different fluid/plate arrangements: —,  $Nu_\infty = Nu_\infty Ra^{-2/7}$ ;  $\cdots$ ,  $Nu^* = Nu^* (Ra^*)^{-2/7}$  and ---,  $Nu = Nu Ra^{-2/7}$ ; all the curves are plotted up to the limit  $R_f/R_p = 10$ . (a) Mercury and copper ( $\lambda_w/\lambda_f = 401/8.65$ ); (b) water and copper at ambient temperature ( $\lambda_w/\lambda_f = 401/0.63$ ); (c) cryogenic gaseous helium and oxygen free copper ( $\lambda_w/\lambda_f = 1000/0.087$ ).  $Nu_\infty = 0.233$  for panels (b) and (c),  $Nu_\infty = 0.116$  for panel (a) according to the data for mercury.  $e/h = 0.05$  for all cases. The quantity  $Nu^*$  is plotted against  $Ra^*$  computed with the corrected temperature difference  $\Delta$  instead of  $\Delta_T$ .

$R_f/R_p \rightarrow 2$  might be only an artifact of the empirical fit of Fig. 11(a). As a matter of fact, with the data available from Fig. 11, we can consider the fits for  $Nu/Nu_\infty$  and  $Nu^*/Nu_\infty$  reliable up to  $R_f/R_p \approx 10$  while further investigation would be necessary to assess their behavior for smaller values.

Once again, the distinction between  $Nu$ ,  $Nu^*$ , and  $Nu_\infty$  allows us to clarify that in an experiment the Nusselt number can differ from the ideal value for two reasons: the first is that the temperature difference  $\Delta_T$  applied to the set up is bigger than that applied to the fluid layer ( $\Delta$ ). The second reason is given by the plume dynamics modified by the finite heat capacity and thermal conductivity of the plates. The first point gives the difference between  $Nu$  and  $Nu^*$  and this can be simply corrected by accounting for the temperature drop in the plates, the second contribution, in contrast, is the difference between  $Nu^*$  and  $Nu_\infty$  and it can only be corrected by models like that of Fig. 11.

Given the good predictive capability of the curve in Fig. 11 and its robustness over the parameter variation ( $2 \times 10^6 \leq Ra \leq 2 \times 10^{10}$ ,  $1 \leq \lambda_w/\lambda_f \leq 10^4$ ,  $0.01 \leq e/h \leq 0.5$ , and  $10^{-2} \leq D \leq 10^2$ ) we can try to speculate about its consequences for high-Rayleigh number laboratory experiments. Since very accurate laboratory experiments can have error bars as low as 2%,<sup>30</sup> we can fix the threshold value of  $R_f/R_p$  such that it results  $Nu/Nu_\infty \approx 0.98$ , yielding  $(R_f/R_p)_{th} \approx 300$ . Assuming a plate thickness  $e/h = 0.05$ , for cryogenic gaseous helium and oxygen free copper, we have  $\lambda_w h / (Nu \lambda_f e) < (R_f/R_p)_{th}$  for  $Nu > 6733$  which happens at  $Ra > 10^{15}$ . On the other hand for standard copper and pure water at ambient temperature the threshold is exceeded for  $Nu > 40$  occurring at  $Ra > 2 \times 10^8$ , while for copper and mercury this happens for  $Nu \geq 3$ , which is around  $Ra \approx 10^5$  in a  $\Gamma = 1/2$  cell! When the Rayleigh number is increased beyond the limiting value, the growth of the Nusselt number is partially reduced according to the curves of Fig. 11 and an apparent reduction of the growth rate can be observed. An example is given in Fig. 12 where it has been assumed that the  $Nu_\infty$  vs  $Ra$  is a pure  $2/7$  power law and the behavior of cryogenic gaseous helium, water, and mercury have been computed. Every setup is eventually affected by the finite conductivity of the plate but the effect on water and mercury is particularly severe, thus suggesting that these fluids are not good candidates for experiments in the “ultimate” Rayleigh number regime. Once

again, since the correction factor is not accurate for  $R_f/R_p \rightarrow 0$ , we have plotted the curves in Fig. 12 up to the Rayleigh number yielding  $R_f/R_p \approx 10$ . Both Nusselt numbers  $Nu$  and  $Nu^*$  are reported and they are computed, respectively, with the total temperature difference  $\Delta_T$  and its corrected value; the mismatch between  $Nu^*$  and  $Nu_\infty$  is smaller than that between  $Nu$  and  $Nu_\infty$  according to the different corrections of Fig. 11. It is worth mentioning that in Fig. 12  $Nu^*$  has been plotted against  $Ra^*$  which is also computed using the corrected temperature difference  $\Delta$ ; the fact that the curves  $Nu^*$  vs  $Ra^*$  do not match the curves  $Nu_\infty$  vs  $Ra$  further confirms that the plates effect cannot be totally corrected by changing  $\Delta_T$ .

The best fluid/plate arrangement is cryogenic helium and oxygen free copper since appreciable finite conductivity effects only appear beyond  $Ra > 10^{15}$ . This confirms that the experiments by Refs. 3 and 31 are both unaffected by the finite conductivity problems and their discrepancies cannot be accounted by this effect. Even if this model is not successful in addressing the mismatch of some recent experiments in helium, it can explain the puzzling discrepancy between the published results of experiments in water and those in helium. In fact, most of water experiments find exponents  $d \ln(Nu)/d \ln(Ra) = 0.28 - 0.29$  while the recent high-Ra helium experiments find exponents  $\approx 0.31$ . On the other hand, let  $Nu = a Ra^\beta$ , with the empirical fit of Fig. 11(a) we can easily compute the exponent  $\beta_\infty$  of the corrected Nusselt number  $Nu_\infty$  through

$$\beta_\infty = \frac{d \ln Nu_\infty}{d \ln Ra} = \beta + \frac{\exp^{-C/Ra^{\beta/3}}}{1 - \exp^{-C/Ra^{\beta/3}}} \frac{C\beta}{3 Ra^{\beta/3}}, \quad (8)$$

being  $C = [(\lambda_w h)/(4\lambda_f e a)]^{1/3}$ . The above expression shows that  $\beta_\infty$  is bigger than  $\beta$  and their difference increases with  $Ra$ . Taking, as an example, the fit of Ref. 32 we have  $Nu = 0.1396 Ra^{0.29}$  that, with the properties of copper and water and assuming  $e/h = 0.05$ , it is obtained  $\beta_\infty = 0.29 + 0.022 = 0.312$  at  $Ra = 10^{10}$  ( $R_f/R_p = 28.7$ ) which compare very well with the results in helium. Another interesting consequence of the above formula is that even if  $\beta$  is constant with  $Ra$ ,  $\beta_\infty$  depends on  $Ra$  showing a positive curvature. One of the signatures of the model in Ref. 12 is the curvature of the  $\ln Nu$  vs  $\ln Ra$  curve that at  $Pr = 4$  gives  $\beta_\infty = 0.287$ ,  $\beta_\infty$

$=0.310$ , and  $\beta_\infty=0.338$ , respectively, at  $Ra=10^8$ ,  $10^{11}$ , and  $10^{14}$ . These exponents are perfectly consistent with Eq. (8) which with the fit of Ref. 32 yields  $\beta_\infty=0.294$ ,  $\beta_\infty=0.312$ , and  $\beta_\infty=0.338$ . Similarly to water, the present correction can reconcile the differences between mercury experiments and other published data. The fit of Fig. 11(b) has been used by Sano<sup>29</sup> to correct his experimental data; it is worth mentioning that the correction in Fig. 11(b) was used instead of that in Fig. 11(a), since the thermal conductivities of copper and mercury are not very different and the correction for the temperature drop within the plates is a common practice. Also in this case it was obtained for  $Ra>10^9$  an exponent  $\beta_\infty \approx 1/3$  which is very much in agreement with that of other fluids.

In addition, since the recent high precision experiments aim at testing the Grossmann and Lohse predictions, formula (8) can be used to estimate the requirements of an experimental apparatus in which finite conductivity effects are negligible; in particular if the  $\beta_\infty$  exponent varies by  $\Delta\beta_\infty=0.04$  over 6 Ra-decades the exponent increase can be roughly estimated as  $\delta\beta_\infty=\Delta\beta_\infty/6=0.0067$  per Ra-decade. In order for an experimental apparatus to be able to appreciate this variation, the correction to  $\beta$  in Eq. (8) must be at most a fraction of  $\delta\beta_\infty$ . This requirement introduces an additional threshold Ra that cannot be exceeded if the finite conductivity effects have not to obscure the  $\ln Nu$  vs  $\ln Ra$  curvature. For example, if the correction must be smaller than  $\delta\beta_\infty/2$ , then for copper and water (with  $e/h=0.05$ ) it results in  $Ra \leq 2 \times 10^8$  while for oxygen free copper and cryogenic gaseous helium it results in  $Ra < 10^{15}$  (using the correlation  $Nu=0.124 Ra^{0.309}$  from Ref. 3, and  $e/h=0.05$ ). We wish to stress that in this case the thresholds Rayleigh numbers for  $(Nu_\infty - Nu)/Nu_\infty \leq 0.02$  and the curvature correction of  $\ln Nu$  vs  $\ln Ra$  smaller than  $\delta\beta_\infty/2$  have the same values; this, however, is coincidental and is only due to the arbitrary choices of the differences between  $Nu_\infty$  with  $Nu$  and the curvature corrections. More restrictive precision requirement would give different threshold Rayleigh numbers the smaller of which would be the limit of the experimental apparatus.

In this discussion we have evidenced that, at the moment, the best fluid/plate arrangement is cryogenic helium and oxygen free copper which is unaffected by finite conductivity problems up to  $Ra=10^{15}$ . This limit, although quite high, still is not enough to address some questions related to the elusive ultra hard regime predicted by Ref. 8. This poses the question of how to design higher Rayleigh number experiments without facing the finite conductivity problems and one possibility is described in Appendix B.

#### IV. CLOSING REMARKS

The correction model derived in the present paper is an attempt to account for the effects of the plate thermal properties on the heat transfer in turbulent thermal convection. One of the main results of this study is that the plates are sensitive to the *effective* thermal conductivity of the fluid  $\lambda_{\text{eff}}=Nu \lambda_f$  rather than to the molecular thermal conductivity  $\lambda_f$ . This implies that, since the Nusselt number increases

monotonically with the Rayleigh number, every setup has a maximum Ra that can be attained before finite conductivity effects interfere with the heat transfer. We wish to stress that only part of these effects can be corrected by diminishing the total temperature difference  $\Delta_T$  by the drop occurring within the plates. The reason is in the changes produced in the thermal plume dynamics by the reduced local heat flux at the plate/fluid interface (see Ref. 15 for a more detailed analysis).

Although the range of parameters investigated in this paper is quite wide, still there are factors which have not been explored like the cell aspect ratio  $\Gamma$  and the Prandtl number. Another point which deserves more investigation is the difference between constant temperature and constant heat flux boundary conditions on the “dry” surfaces of the plates. In real laboratory setups the situation is very complex since hot and cold plates have different thicknesses and different heating and cooling systems yielding a hot plate which is well approximated by a constant heat flux surface while the cold plate is better represented by a constant temperature surface.<sup>16</sup> In addition the presence of auxiliary devices (like flanges, thermal links, sealing rings, etc.) could lead to an effective plate thickness different from its nominal value. A further point deserving some caution is the possibility of quantitatively applying the present correction to convective regimes different from those simulated here; in particular the two extreme cases are liquid metals soft/hard convection (where thermal plumes hardly form) and the ultimate regime (plume dominated).

Despite the above mentioned problems, the correction proposed in this paper (Fig. 11) worked very well for a recent experiment where the heat transfer measurements were systematically smaller than the theoretical prediction of Ref. 12 with a difference which increased with Ra and it became as large as 11% at  $Ra=10^{11}$ .<sup>33</sup> In particular, the cell was cylindrical of the unity aspect ratio ( $\Gamma=1$ ) and it was filled with pure water at a mean temperature  $T=313$  K ( $Pr=4.38$ ). The lower plate was a 3.5 cm thick aluminum block while the top plate was more complicated since it was 2.54 cm thick but it contained channels carrying the cooling water; the thickness below the bottom of these channels was 0.8 cm. By assuming an effective plate thickness of 0.9 cm (equal for top and bottom plate) it has been possible to account for all the mismatch between measurements and theory<sup>12</sup> for a range of Rayleigh numbers in between  $Ra=10^9$  and  $10^{11}$ .

Further work is needed to understand the effects of the unexplored parameters, however, the fact that for the experiment by Nikolaenko and Ahlers<sup>33</sup> the reasonable value  $e_{\text{eff}}=0.9$  cm (in between 3.5 cm and 0.8 cm, respectively of the lower and upper plates) could absorb all the difference between experiments and theory suggests that the correction model proposed in this paper captures the essential physics.

Before concluding this paper we wish to shortly mention the results obtained more than 150 years ago by Péclet<sup>34</sup> in an experiment on the thermal conductivity of metals. He used a device with a continuously stirred fluid bounded by metal plates whose thickness  $e$  could be changed. He reported that the heat flux increased with the stirring of the

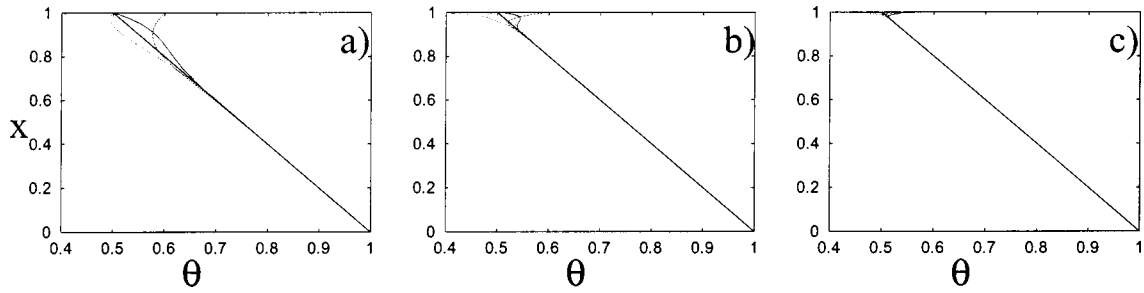


FIG. 13. Temperature profiles across the plate thickness; the thick solid line in each panel is the time averaged solution, the other lines are instantaneous profiles every 1/4 of period. (a)  $Ra=2 \times 10^{13}$  and  $R_f/R_p=1440$ ; (b)  $Ra=2 \times 10^{15}$  and  $R_f/R_p=347$ ; (c)  $Ra=2 \times 10^{17}$  and  $R_f/R_p=83.57$ . The results have been obtained assuming  $\theta_0=1$ ,  $\theta_e=0.5$ ,  $\theta_p=0.1$ ,  $e=1$ ,  $e/h=0.05$ , and  $Nu=0.124 Ra^{0.309}$ .

fluid, increased for decreasing  $e$  and it became independent of the plate thickness only when it was below a threshold value. Péclet indicated this behavior as an “anomaly” of the thermal conductivity of the metals  $\lambda_w$  since, for large plate thicknesses, its value turned out to be dependent on  $e$ . These observations, however, can be interpreted with the help of Fig. 11 since Péclet’s experiment implied forced heat convection and for decreasing  $e$  the value  $R_f/R_p$  increases together with  $Nu/Nu_\infty$ . Only when  $R_f/R_p$  exceeds the value  $R_f/R_p \approx 300$  the ratio  $Nu/Nu_\infty$  becomes indistinguishable from unity and the heat transfer is independent of  $e$ .

## ACKNOWLEDGMENTS

The preparation of this paper largely benefitted from discussions at the workshop on “High Rayleigh Number Thermal Convection” held in Leiden, June 10–20, 2003. The author is indebted to all the participants, and in particular to G. Ahlers, B. Castaing, R. Ecke, R. Kerr, D. Lohse, J. Niemela, P. Roche, M. Sano, K. Sreenivasan, and E. Villermaux for the suggestions and remarks received. The paper was prepared with the financial support of CEMeC of Politecnico di Bari. The technical support of CASPUR (Consorzio Interuniversitario per le Applicazioni di Supercalcolo Per Universitàe Ricerca) provided by Dr. F. Massaioli and Dr. G. Amati is gratefully acknowledged.

## APPENDIX A

In this appendix, by a simplified one-dimensional model problem, an argument is given for the presence of the ratio of the thermal conductivities  $\lambda_w/\lambda_f$  in the correction factor of Fig. 11 rather than the ratio of the thermal diffusivities  $k_w/k_f$  as it would be expected given the problem unsteadiness.

Consider the hot plate of the convective cell in Fig. 2 which on the bottom  $x=0$  has a constant temperature while on the top  $x=e$  the temperature boundary condition is time dependent owing to the action of the unsteady flow sweeping the surface; if we neglect the horizontal space variations, being  $e$  the plate thickness, we have  $\theta(0,t)=\theta_h$  and  $\theta(e,t)=\theta_e+\theta_p \exp^{i\omega t}$ , where  $\theta_e$  is the mean temperature at the fluid/plate interface,  $\theta_p$  is the amplitude of the temperature perturbation, and  $\omega=2\pi/\tau$  gives the flow-induced time variation with period  $\tau$ . The time dependent one-dimensional temperature profile across the plate thickness obeys to

$$\frac{\partial \theta}{\partial t} = \frac{1}{Pe} \frac{\partial^2 \theta}{\partial x^2} \quad (9)$$

with  $Pe$  the Péclet number defined as  $Pe = \sqrt{Pr} Ra k_f / k_w$ . For the given boundary conditions the above equation yields

$$\theta(x,t) = \theta_h + (\theta_e - \theta_h) \frac{x}{e} + \theta_p \frac{\exp^{-i\beta x} - \exp^{i\beta x}}{\exp^{-i\beta e} - \exp^{i\beta e}} \exp^{i\omega t}, \quad (10)$$

being  $-\beta^2 = i\omega Pe$ . This solution has been plotted assuming that the plate is pure copper and the above fluid cryogenic helium; as a consequence the time scale of the flow can be taken as the time between two successive plume detachments  $\tau \approx \sqrt{Ra Pr} / (4 Nu^2)$ , while  $\theta_p$  was considered independent of  $Ra$  since each thermal boundary layer always supports half of the total temperature difference and the generation of a plume implies the detachment of a portion of boundary layer. The results are in Fig. 13 for three different Rayleigh numbers.

It is worth noting that as the Rayleigh number is increased above  $Ra \approx 2 \times 10^{15}$  the correction parameter decreases below the threshold value  $R_f/R_p \approx 300$  and the difference between  $Nu$  and  $Nu_\infty$  becomes relevant. In this regime, however, according to the panels (b) and (c) of Fig. 13 most of the plate thickness is in a steady regime with the temperature unsteadiness that affects only a very thin region adjacent to the upper boundary. This might explain why the correction parameter  $R_f/R_p = \lambda_w h / (\lambda_f e Nu)$  contains the plate thermal conductivity  $\lambda_w$  although the unsteady nature of the phenomenon would suggest the use of the thermal diffusivity  $k_w$ . On the other hand it must be stressed that even if the penetration depth ( $1/\beta$ ) of the temperature oscillation is much smaller than the plate thickness ( $e$ ) this does not necessarily imply that the heat transfer obeys to the steady state temperature distribution. In fact, as seen in Sec. III A, there is a two-way coupling between the plume generation and the plate heat transfer and the temperature distribution at the fluid/plate interface is determined by the interaction of both.

On the side we note that considering  $\theta_p$  independent of  $Ra$  is only an approximation although it can explain the correction parameter of Fig. 11(a); in fact, if  $\Delta^*$  is the temperature difference across the fluid we can write  $\lambda_f \Delta^* Nu / h = \lambda_w \theta_p / e$  which gives  $\Delta^* / \theta_p = (\lambda_w h) / (\lambda_f e Nu)$  (Ref. 35).

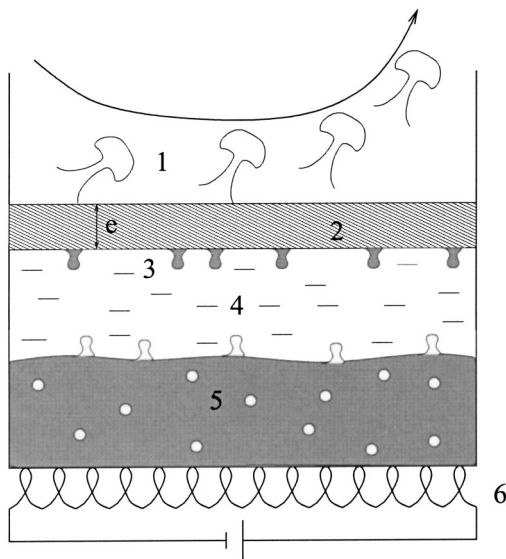


FIG. 14. Sketch of the “heat pipe”: (1) convective fluid layer; (2) metal plate of thickness  $e$ ; (3) condensing vapor; (4) fluid vapor; (5) boiling liquid; (6) heating device for the liquid.

In a recent paper the same authors argue that the temperature fluctuations in the bulk ( $\delta^*$ ) are the relevant parameter rather than  $\Delta^*$  and this yields the correction factor in the form  $(\lambda_w h)/(\lambda_f e \text{Re Pr})$  instead of  $(\lambda_w h)/(\lambda_f e \text{Nu})$ . A relevant difference could be that the present correction has been computed for constant temperature boundary conditions while in that paper constant heat flux was considered for the plates; both results should be checked with ad hoc experiments.

## APPENDIX B

We have seen in the paper that using the traditional arrangement for the heating and cooling plates, any experimental apparatus has a threshold Rayleigh number beyond which the plates are not enough conductive to provide the flow with the required heat. Although the maximum Rayleigh number depends on material properties and flow condition, we have estimated at best, for cryogenic helium and oxygen free copper, a threshold of  $\text{Ra} = 10^{15}$  which still is not high enough to answer several questions about the physics of convective turbulence. One possibility to push this limit further up could be a different heating device (Fig. 14) for the hot plate known as “heat pipe.”<sup>36</sup> It consists of a boiling liquid, with the temperature adjustable by controlling its absolute pressure, whose vapor is allowed to condense on the lower side of a thin and highly conducting metal plate. If on the upper side of this plate convective phenomena are occurring and an intense local heat flux is needed, from the lower side a larger amount of vapor will condense thus preventing the local plate temperature from decreasing. This device gives an extremely stable and uniform temperature distribution on the plate surface, provided this is thin enough to avoid all the phenomena described in this paper. In principle, the plate thickness could be reduced to vanishing values even if practical considerations (the plate must sustain itself and it should not deform under the weight of the upper fluid or the pressure difference between upper and lower sides) suggest

to maintain this thickness finite. In this case, however, since the temperature of the lower side of the plate is exactly constant, as requested by the phase change process, the correction derived in the present paper could be applied without approximations. On the other hand, such a good heating system requires an equally good cooling system for the cold plate and the heat pipe is apparently not very efficient owing to the “film boiling” phenomenon which prevents the adequate heat transfer between the cold plate and the boiling liquid.<sup>29</sup>

<sup>1</sup>X. Z. Wu and A. Libchaber, “Scaling relations in thermal turbulence: The aspect-ratio dependence,” *Phys. Rev. A* **45**, 842 (1992).

<sup>2</sup>R. J. Goldstein and S. Tokuda, “Heat transfer by thermal convection in high Rayleigh numbers,” *Int. J. Heat and Mass Transfer* **23**, 738 (1979).

<sup>3</sup>J. J. Niemela, L. Skrbek, K. R. Sreenivasan, and R. J. Donnelly, “Turbulent convection at very high Rayleigh numbers,” *Nature (London)* **404**, 837 (2000).

<sup>4</sup>X. Chavanne, F. Chillà, B. Chabaud, B. Castaing, and B. Hébral, “Turbulent Rayleigh–Bénard convection in gaseous and liquid He,” *Phys. Fluids* **13**, 1300 (2001).

<sup>5</sup>J. A. Glazier, T. Segawa, A. Naert, and M. Sano, “Evidence against ‘ultra-had’ thermal turbulence at very high Rayleigh numbers,” *Nature (London)* **398**, 307 (1999).

<sup>6</sup>B. Castaing, B. Chabaud, B. Hébral, X. Chavanne, P. Chanal, and P. Roche, “Cryogenic turbulence experiments,” *Advances in Turbulence VIII Proceedings of the 8th European Turbulence Conference*, edited by C. Dopazo (CIMNe, Barcelona, 2000), p. 125.

<sup>7</sup>S. Chaumat, B. Castaing, and F. Chillà, “Rayleigh–Bénard cells: Influence of the plate properties,” *Advances in Turbulence IX Proceedings of the 9th European Turbulence Conference*, edited by I. P. Castro and P. E. Hancock (CIMNe, Barcelona 2002), id:46,1.

<sup>8</sup>R. H. Kraichnan, “Turbulent thermal convection at arbitrary Prandtl number,” *Phys. Fluids* **5**, 1374 (1962).

<sup>9</sup>G. Ahlers, “Effect of sidewall conductance on heat-transport measurements for turbulent Rayleigh–Bénard convection,” *Phys. Rev. E* **63**, 015303 (2001).

<sup>10</sup>P. E. Roche, B. Castaing, B. Chabaud, B. Hébral, and J. Sommeria, “Side wall effects in Rayleigh–Bénard experiments,” *Eur. Phys. J. B* **24**, 405 (2001).

<sup>11</sup>R. Verzicco, “Sidewall finite conductivity effects in confined turbulent thermal convection,” *J. Fluid Mech.* **473**, 201 (2002).

<sup>12</sup>S. Grossmann and D. Lohse, “Prandtl and Rayleigh number dependence of the Reynolds number in turbulent thermal convection,” *Phys. Rev. E* **66**, 016305 (2002).

<sup>13</sup>H. Schlichting, *Boundary Layer Theory* (McGraw–Hill, New York, 2000).

<sup>14</sup>J. Niemela and P. Roche (personal communication).

<sup>15</sup>J. C. R. Hunt, A. J. Vrieling, F. T. M. Nieustadt, and H. J. S. Fernando, “The influence of the thermal diffusivity of the lower boundary on eddy motion in convection,” *J. Fluid Mech.* **491**, 183 (2003).

<sup>16</sup>S. Cioni, S. Ciliberto, and J. Sommeria, “Strongly turbulent Rayleigh–Bénard convection in mercury: Comparison with results at moderate Prandtl number,” *J. Fluid Mech.* **335**, 111 (1997).

<sup>17</sup>R. Verzicco and P. Orlandi, “A finite-difference scheme for three-dimensional incompressible flow in cylindrical coordinates,” *J. Comput. Phys.* **123**, 402 (1996).

<sup>18</sup>E. A. Fadlun, R. Verzicco, P. Orlandi, and J. Mohd-Yusof, “Combined immersed-boundary/finite-difference methods for three-dimensional complex flow simulations,” *J. Comput. Phys.* **161**, 35 (2000).

<sup>19</sup>R. Verzicco and R. Camussi, “Numerical experiments on strongly turbulent thermal convection in a slender cylindrical cell,” *J. Fluid Mech.* **477**, 19 (2003).

<sup>20</sup>P. N. Swartzrauber, “A direct method for the discrete solution of separable elliptic equations,” *SIAM (Soc. Ind. Appl. Math.) J. Numer. Anal.* **11**, 1136 (1974).

<sup>21</sup>Z. A. Daya and R. E. Ecke, “Does turbulent convection feel the shape of the container?” *Phys. Rev. Lett.* **87**, 184501 (2001).

<sup>22</sup>R. Verzicco, “Turbulent thermal convection in a closed domain: Viscous boundary layer and mean flow effects,” *Eur. Phys. J. B* **35**, 133 (2003).

<sup>23</sup>A. Umeura and F. Busse, “Axisymmetric convection at large Rayleigh and infinite Prandtl number,” *J. Fluid Mech.* **208**, 459 (1989).

- <sup>24</sup>R. Verzicco and R. Camussi, "Prandtl number effects in convective turbulence," *J. Fluid Mech.* **383**, 55 (1999).
- <sup>25</sup>B. Castaing, G. Gunaratne, F. Heslot, L. Kadanoff, A. Libchaber, S. Thomae, X. Z. Wu, S. Zaleski, and G. Zanetti, "Scaling of hard thermal turbulence in Rayleigh–Bénard convection," *J. Fluid Mech.* **204**, 1 (1989).
- <sup>26</sup>J. J. Niemela and K. R. Sreenivasan, "Confined turbulent convection," *J. Fluid Mech.* **481**, 355 (2003).
- <sup>27</sup>P. E. Roche, B. Castaing, B. Chabaud, and B. Hébral, "Prandtl and Rayleigh numbers dependencies in Rayleigh–Bénard convection," *Europhys. Lett.* **58**, 693 (2002).
- <sup>28</sup>A. Naert, T. Segawa, and M. Sano, "High-Reynolds-number thermal turbulence in mercury," *Phys. Rev. E* **56**, 1302 (1997).
- <sup>29</sup>M. Sano (personal communication).
- <sup>30</sup>G. Ahlers and X. Xu, "Prandtl number dependence of heat transport in turbulent Rayleigh–Bénard convection," *Phys. Rev. Lett.* **86**, 3320 (2001).
- <sup>31</sup>X. Chavanne, F. Chillà, B. Castaing, B. Hébral, B. Chabaud, and J. Chaussy, "Observation of the ultimate regime in Rayleigh–Bénard convection," *Phys. Rev. Lett.* **79**, 3648 (1997).
- <sup>32</sup>Y.-B. Xin, K.-Q. Xia, and P. Tong, "Measured velocity boundary layers in turbulent convection," *Phys. Rev. Lett.* **77**, 1266 (1996).
- <sup>33</sup>A. Nikolaenko and G. Ahlers, "Nusselt number measurements for turbulent Rayleigh–Bénard convection," *Phys. Rev. Lett.* **91**, 084501 (2003).
- <sup>34</sup>E. Pécelet, "Sur la détermination des coefficients de conductibilité des métaux par la chaleur," *Ann. Chim. Phys.* **3**, 107 (1841).
- <sup>35</sup>F. Chillà, F. Rastello, S. Chaumat, and B. Castaing (personal communication).
- <sup>36</sup>G. Ahlers and R. Ecke (personal communication).